

## NUMERICAL INVESTIGATION OF TIP GEOMETRY ON THE TIP-CLEARANCE FLOW FEATURES OF A PUMP-JET PROPULSOR

Xue-Qin Ji, Xiao-Qian Dong\*, Wei Li, Chen-Jun Yang, Francis Noblesse

(State Key Laboratory of Ocean Engineering,  
Collaborative Innovation Center for Advanced Ship and Deep-Sea Exploration,  
Shanghai Jiao Tong University, Shanghai 200240, China)

\*Corresponding author: xiaoqiandong0330@sjtu.edu.cn (X.-Q. D.)

**Key words:** Pump-jet; Tip-clearance flow; CFD; Uncertainty

**Abstract:** The numerical simulation for pump-jet propulsors is based on the solution of the Reynolds-Averaged Navier-Stokes (RANS) equations using a two-layer realizable  $k-\varepsilon$  model for turbulence closure. The computational domain is discretized into block-structured hexahedral cells. To establish a reliable simulation model, the numerical uncertainties are evaluated according to the procedure recommended by the 28<sup>th</sup> International Towing Tank Conference (ITTC). Three sets of grids, with a uniform refinement ratio, are generated for a generic pump-jet propulsor at model scale using the grid generator ICEM CFD 17.2, and the flow simulations are carried out using the software package STAR-CCM<sup>+</sup>. The tip-clearance flow features are numerically investigated for varied thickness and rake profiles of the sections close to the rotator tip. It is shown that the tip geometry has significant influence on the tip vortex.

### 1 INTRODUCTION

The pump-jet propulsor is receiving increased attention for underwater vehicles due to the advantage of low acoustic signature. Lots of experimental and numerical research has been done. Suryanarayana *et al.* [1,2] carried out several experiments in a wind tunnel to evaluate the hydrodynamic performance of a pump-jet propulsor. Ivanell *et al.* [3] used the Computational Fluid Dynamics (CFD) method to simulate the hydrodynamic performance of a torpedo equipped with the pump-jet propulsion system. The numerical results are in good agreement with the experimental data. Cheah *et al.* [4] simulated the complex flow in a centrifugal pump numerically. Pan *et al.* [5] calculated the steady hydrodynamic performance by adopting the RANS method and the  $SST k-\omega$  turbulence model. The predicted open water performance indicates that the pump-jet propulsor has a high propulsive efficiency and an ideal balance of performance. Lu *et al.* [6] predicted the unsteady cavitation performance of the pump-jet propulsor for a UUV using Z-G-B cavitation model. The inception and geometry of cavitation were well predicted. Cavitation inception and radiated noise seem to be closely related to the strength of the vortical flow that initiates in the clearance between the rotator tips and the duct. With the development of computer hardware capacity and CFD software technology, the tip-clearance flow can be simulated with higher resolution and fidelity. Lu *et al.* [7] employed the CFD method to investigate the tip-clearance flow characteristics of a pump-jet propulsor and the influence of the tip clearance size on the characteristics of cavitation. The research presents the formation and development of the tip-clearance flow and concludes that the tip-clearance size has a direct influence on the

cavity distribution and the cavitation area enlarges with the increase of the tip-clearance. Qin *et al.* [8] investigated the effect of different tip clearances on the hydrodynamic performance of the pump-jet propulsor numerically. The results show that the low-pressure area gradually moves from the leading edge to the trailing edge and the affected areas of pressure and tip-leakage vortex increase with the increase of the tip clearance, which leads to a reduction in the propulsive efficiency. Gu *et al.* [9] analyzed the impact of the duct camber on a pump-jet propulsor by changing the camber ratio of the duct section. The analysis shows that the propulsive efficiency and the effective work range of the pump-jet propulsor are significantly improved as the camber increases. The research work in wind turbine area [10,11] indicates that the tip vanes. Li *et al.* [12] further investigated the influence of the width and thickness of the tip vanes on the hydrodynamic performance and fluctuating pressure of the pump's shroud. The results show that the fluctuating pressure of the pump's shroud decreases initially but increases afterwards as the widths increase. To the authors' knowledge, there are few studies on the influence of the rotator tip geometry on the tip-clearance flow in a pump-jet propulsor. In this paper, different tip geometries are investigated via viscous flow CFD simulations. The differences in tip-clearance flow and hydrodynamic performance are analyzed by changing the thickness and rake in the tip region.

## 2 NUMERICAL METHOD

The numerical simulation is based on the solution of the Reynolds-Averaged Navier-Stokes (RANS) equations governing the incompressible single-phase fluid flow. The two-layer realizable  $k$ - $\varepsilon$  model is employed to simulate the turbulent flow. The two-layer approach proposed by Rodi *et al.* [13] deals with either low-Reynolds-number type grids or wall-function type grids respectively for  $y^+ \sim 1$  or  $y^+ > 30$ . In this paper, we choose to resolve the viscous sub-layer flow by using very thin wall-bounded grid layers to ensure that the body-surface  $y^+$  is in the order of 1. Shih *et al.* [14] found that the realizable  $k$ - $\varepsilon$  model performs better than the standard  $k$ - $\varepsilon$  model. The governing equations are discretized with second-order schemes both in space and time and solved by the SIMPLE algorithm. The hydrodynamic interactions of the rotor with the stator and the duct are treated with both steady and unsteady flow models. The RANS simulations are carried out using the CFD software STAR-CCM<sup>+</sup>.

## 3 NUMERICAL SIMULATION OF PUMP-JET PROPULSOR

### 3.1 Propulsor geometry

The prototype pump-jet propulsor, named as PJP-1, consists of a five-bladed rotor, a seven-bladed pre-swirl stator and a decelerating duct. Figure 1 shows the geometric model of the pump-jet propulsor. The diameter of the rotor,  $D_R$ , is 293.81 mm and the clearance between the rotor blade tips and the duct is 1 mm. The chord length and the maximum thickness of the rotor blade tips are 60.57 mm and 4.14 mm, respectively.

To investigate the influence of blade tip geometry on the tip-clearance flow, another propulsor, named as PJP-2, is designed by changing the thickness and rake profiles of the PJP-1 in the region from  $0.95 r_R$  to  $1.0 r_R$ , where  $r_R$  denoted the radius of the tip section at the

rotator blade disk position,  $r_R=D_R/2$ . All the other geometric parameters of the two propulsors are kept identical. The amount of changes in section thickness and rake are determined respectively by

$$\Delta t(r) = \Delta t_m \left( 20 \frac{r}{r_R} - 19 \right)^2 \quad (0.95 \leq r/r_R \leq 1) \quad (1)$$

and

$$\Delta x(r) = \Delta x_m \left( 20 \frac{r}{r_R} - 19 \right)^2 \quad (0.95 \leq r/r_R \leq 1) \quad (2)$$

Where  $\Delta t_m$  and  $\Delta x_m$  denote the maximum amount of changes in section thickness and rake, respectively. For the PJP-2,  $\Delta t_m$  is equal to 20% of  $t_{tip}$ , the maximum thickness of PJP-1's tip section, and  $\Delta x_m$  is equal to 0.75% of  $D_R$ . Figure 2 and Figure 3 show the changes in thickness and rake at the blade tip, respectively. Figure 4 compares the 3-D geometries of a rotor blade in the tip region before and after the thickness and rake are changed.

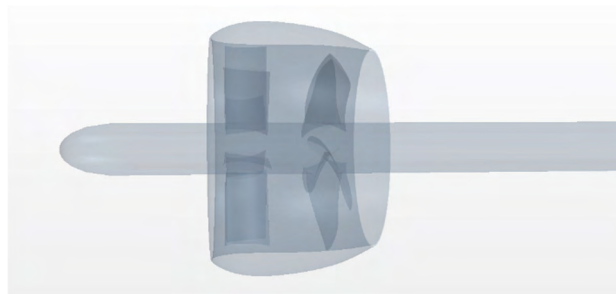


Figure 1: The geometric model of the pump-jet propulsor.

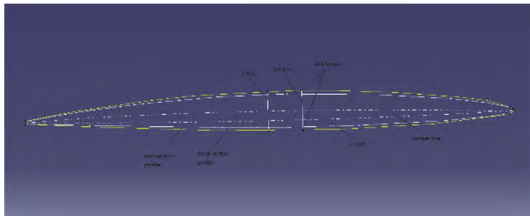


Figure 2: Change in the thickness at the blade tip.

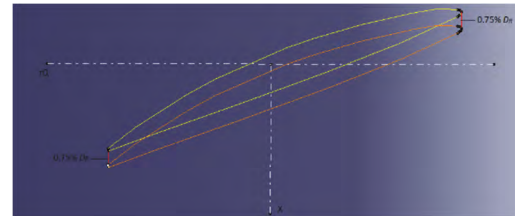


Figure 3: Change in rake at the blade tip.

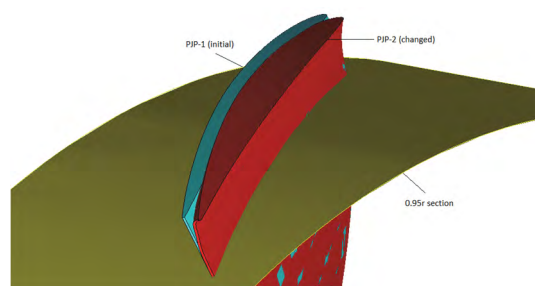
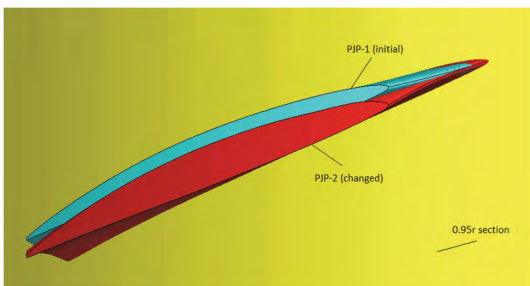


Figure 4: Comparison of the geometries of a rotor blade in the tip region of PJP-1 and PJP-2.

### 3.2 Computational domain and boundary conditions

Figure 5 shows the computational domain, a cylinder surrounding the pump-jet propulsor which is  $15D_R$  in length and  $5.9D_R$  in diameter. The velocity inlet is located at  $4.7D_R$  upstream of the rotor blade disk, and the pressure outlet is located at  $10.3D_R$  downstream of the rotor blade disk. The cylinder surface of the domain is set as the velocity inlet. The computational domain is divided into a static sub-domain and a rotating sub-domain. The coordinate system of the rotating sub-domain is attached to the rotor, while the static sub-domain is earth-fixed. The lateral boundary of the rotating sub-domain is the inner surface of the duct and the length is  $0.38D_R$ .

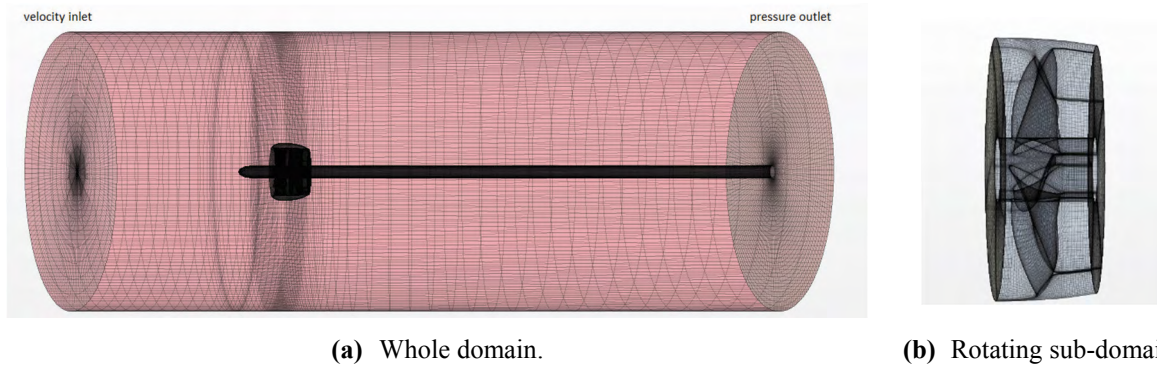


Figure 5: The computational domain.

### 3.3 Computational grid

The computational domain for the pump-jet propulsor is discretized into block-structured hexahedral cells, using the grid generator ICEM CFD 17.2. The grids are generated for the flow passage containing a single stator blade in the static sub-domain, see Figure 6 (left), and for the flow passage containing a single rotor blade in the rotating sub-domain, see Figure 6 (right). Then the single-passage grid blocks are copied, rotated around the rotor shaft axis, and combined to form the whole flow passage shown in Figure 5. Figure 7 illustrates the grid topology around rotor blade sections and the grids in the tip clearance region. The area around the rotor blade surfaces is discretized with C-type grids and the area between adjacent blades is discretized with L-type grids.

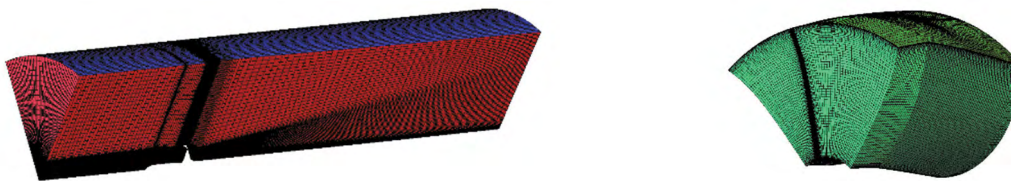
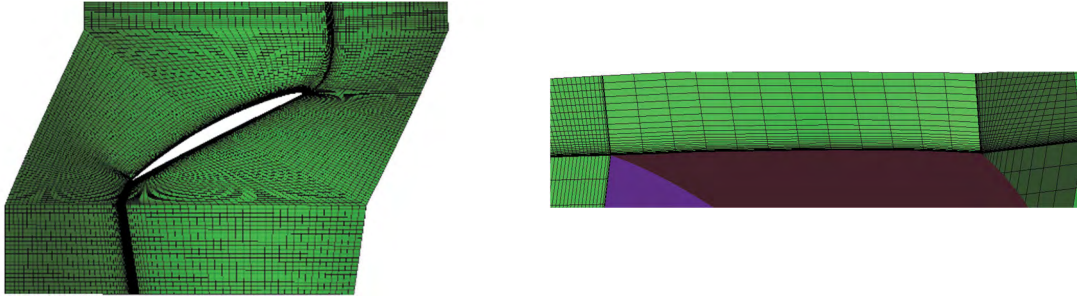


Figure 6: The single-passage grids in the static sub-domain (left) and the rotating sub-domain (right).



**Figure 7:** The grid topology around a rotor blade section (left) and the grids structure in the tip clearance at mid-chord (right).

To perform the analysis of numerical simulation uncertainties, three sets of grids are generated with a uniform refinement ratio. The grid refinement ratio,  $r_G$ , is defined as

$$r_G = \Delta h_2 / \Delta h_1 = \Delta h_3 / \Delta h_2 = \sqrt{2} \quad (3)$$

where  $h_1$ ,  $h_2$  and  $h_3$  denote, respectively, the sizes of fine grid  $G_1$ , medium grid  $G_2$ , and coarse grid  $G_3$ . The grid refinement ratio is set as  $\sqrt{2}$  for the three sets of grids.

## 4 RESULTS AND DISCUSSIONS

To establish a reliable simulation model, the numerical uncertainties are evaluated firstly according to the unsteady flow simulation results of the PJP-1. In addition, steady flow simulations are also carried out to compare the numerical and experimental open water performances. Through the uncertainty analysis and the validation against physical model experiments, the grid parameters suitable for investigating the tip-clearance flow are determined. The tip-clearance flow features and hydrodynamic performance are compared between PJP-1 and PJP-2 to study the influence of tip geometry on the tip-clearance flow.

### 4.1 Numerical uncertainty analysis for PJP-1

The uncertainty analysis consists of verification and validation based on the procedure recommended by the 28<sup>th</sup> International Towing Tank Conference (ITTC) [15]. In this paper, the uncorrected approach is adopted to evaluate the numerical uncertainties in the trust coefficient ( $K_{TR}$ ) and torque coefficient ( $K_Q$ ) of the rotor, simulated with the unsteady flow model, at the advance coefficient ( $J$ ) of 0.75 and 0.9.

Verification is the process for estimating the uncertainty in numerical simulations. The numerical uncertainty  $U_{SN}$  is expressed as

$$U_{SN}^2 = U_I^2 + U_G^2 + U_T^2 + U_P^2 \quad (4)$$

where  $U_I$ ,  $U_G$ ,  $U_T$  and  $U_P$ , respectively, denote the uncertainties due to iteration, grid size, time step and other parameters. The  $U_G$  and  $U_T$  can be replaced by a combined uncertainty  $U_{GT}$  due to spatial and temporal discretizations (Qiu *et al.* [16]). Then the numerical uncertainty is expressed as

$$U_{SN}^2 = U_I^2 + U_{GT}^2 + U_P^2 \quad (5)$$

The iteration uncertainty  $U_I$  is estimated as the difference of the averaged simulation results in the last two revolutions of the rotor.

In this paper,  $U_P$  is not investigated and will be neglected.

For the verification based on three solutions, the convergence ratio  $R$  is defined as

$$R = \varepsilon_{21} / \varepsilon_{32} = (S_2 - S_1) / (S_3 - S_2) \quad (6)$$

where  $S_1$ ,  $S_2$  and  $S_3$  denote the simulation results, respectively, with fine, medium and coarse grid and time step sizes. The convergence is monotonic when  $0 < R < 1$ .

According to the Richardson Extrapolation (RE) approach, the one-term estimates of the error,  $\delta_{RE}^*$  and the observed order of accuracy,  $p$ , are calculated respectively as

$$\delta_{RE}^* = \frac{\varepsilon_{21}}{r^p - 1} \quad (7)$$

$$p = \frac{\ln(\varepsilon_{32} / \varepsilon_{21})}{\ln(r)} \quad (8)$$

where  $r$  denotes the uniform parameter refinement ratio. In this paper, the refinement ratios for grid and time step sizes are both set as  $\sqrt{2}$  because the governing equations are discretized with second-order schemes both in space and time, which means  $r = r_G = r_T = \sqrt{2}$ .

The correction factor,  $C$ , is defined as

$$C = \frac{r^p - 1}{r^{p_{est}} - 1} \quad (9)$$

where  $p_{est}$  is an estimate for the limiting order of accuracy of the first term as spacing sizes go to zero and the asymptotic range is reached, *i.e.*  $C \rightarrow 1$ . In this paper,  $p_{est}$  is taken as 2.

According to the uncorrected approach, the  $U_{GT}$  is estimated as

$$U_{GT} = \begin{cases} [9.6(1-C)^2 + 1.1] |\delta_{RE}^*|, & |1-C| < 0.125 \\ (2|1-C|+1) |\delta_{RE}^*|, & |1-C| \geq 0.125 \end{cases} \quad (10)$$

Validation is the process for assessing simulation modelling uncertainty by using benchmark experimental data. The validation uncertainty  $U_V$  is defined as

$$U_V^2 = U_D^2 + U_{SN}^2 \quad (11)$$

where  $U_D$  denotes experimental uncertainty. Due to the lack of experimental uncertainty data, the experimental uncertainty  $U_D$  is assumed to be 2.5%. The comparison error  $E$ , the difference between experimental data  $D$  and simulation results  $S$  of fine grid, is compared to the validation uncertainty  $U_V$ .

Table 1 shows the key parameters of computational grids, where GT1, GT2, and GT3 denote the grid models using fine, medium, and coarse grid and time-step sizes, respectively. The simulation results and comparison errors corresponding to the three grid models are shown in Table 2.

**Table 1:** Key parameters of the grid models.

Model ID.	Total number of cells (Million)	Time step size	$y^+$ ( $J=0.75$ )		$y^+$ ( $J=0.9$ )	
			back	face	back	face
GT1	37.27	$0.5^\circ$	0.92	0.86	0.92	0.87
GT2	12.53	$0.707^\circ$	1.28	1.18	1.29	1.19
GT3	4.93	$1^\circ$	1.77	1.68	1.78	1.65

**Table 2:** Simulation results and comparison errors of grid models.

Model ID.	$J=0.75$				$J=0.9$			
	$K_{TR}$	$E$ (%D)	$10K_Q$	$E$ (%D)	$K_{TR}$	$E$ (%D)	$10K_Q$	$E$ (%D)
GT1	0.5321	-0.34	1.0221	2.28	0.5059	2.01	0.9897	4.27
GT2	0.5342	0.05	1.0254	2.61	0.5089	2.62	0.9944	4.77
GT3	0.5426	1.62	1.0360	3.67	0.5183	4.51	1.0067	6.05

The iteration uncertainties are all lower than 0.012% and negligibly smaller than  $U_{GT}$ , hence  $U_{SN} \approx U_{GT}$ . The key parameters and uncertainties are presented in Table 3. The validation is successfully achieved at the  $U_V$  level of 2.5-2.7%, except for the torque coefficient ( $K_Q$ ) at  $J=0.9$ .

**Table 3:** Results of the uncertainties and comparison errors.

$J$	<i>Experiment</i>	$R$	$p$	$C$	$U_{SN}$ (%D)	$U_V$ (%D)	$ E $ (%D)	
0.75	$K_{TR}$	0.5339	0.25	4.02	3.02	0.7	2.59	0.34
	$10K_Q$	0.9993	0.30	3.45	2.31	0.5	2.55	2.28
0.9	$K_{TR}$	0.4959	0.33	3.24	2.07	0.9	2.66	2.01
	$10K_Q$	0.9492	0.39	2.74	1.58	0.7	2.60	4.27

## 4.2 Hydrodynamic performance of PJP-1

Taking computing time into major consideration, GT3 is applied to predict the PJP-1's open water performance by steady and unsteady flow simulation models, although the errors in predicted performance are relatively larger than the other two grid models. Table 4 compares the numerical results with available experimental data, where  $K_{TR}$ ,  $K_{TS}$ , and  $K_{TD}$  denote the thrust coefficients of the rotor, the stator, and the duct, respectively. The open-water efficiency,  $\eta$ , of the propulsor is based on  $K_{TT}$ , the total thrust coefficient of the propulsor, and  $K_Q$ , the torque coefficient of the rotor. The model experiments for the PJP-1 in uniform flows were conducted in the large cavitation tunnel of Shanghai Jiao Tong University in 2018.

**Table 4:** Comparison of the hydrodynamic coefficients of PJP-1 simulated using GT3 with experimental data.

$J$	$K_{TR}$			$K_{TD}$		$K_{TS}$	
	steady	unsteady	experimental	steady	unsteady	steady	unsteady
<b>0.3</b>	0.5722	0.5815	0.6083	0.1393	0.1319	-0.0425	-0.0434
<b>0.5</b>	0.5570	0.5736	0.5826	0.0750	0.0696	-0.0435	-0.0430
<b>0.75</b>	0.5209	0.5426	0.5339	0.0015	-0.0057	-0.0478	-0.0475
<b>0.9</b>	0.4938	0.5183	0.4959	-0.0323	-0.0433	-0.0522	-0.0516
<b>1.1</b>	0.4504	0.4779	0.4316	-0.0666	-0.0805	-0.0603	-0.0589

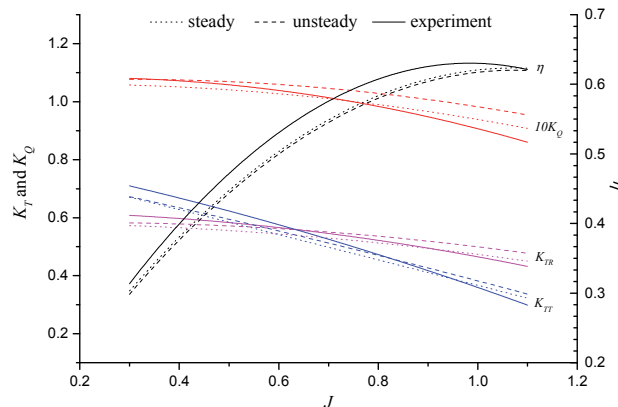
  

$J$	$K_{TT}$			$10K_Q$			$\eta$		
	steady	unsteady	experimental	steady	unsteady	experimental	steady	unsteady	experimental
<b>0.3</b>	0.6690	0.6699	0.7102	1.0565	1.0759	1.0810	0.302	0.297	0.314
<b>0.5</b>	0.5884	0.6002	0.6221	1.0429	1.0722	1.0574	0.449	0.445	0.471
<b>0.75</b>	0.4746	0.4894	0.4993	0.9996	1.0360	0.9993	0.567	0.564	0.593
<b>0.9</b>	0.4093	0.4233	0.4190	0.9654	1.0067	0.9492	0.607	0.602	0.626
<b>1.1</b>	0.3235	0.3385	0.2979	0.9083	0.9547	0.8597	0.623	0.621	0.621

For  $J=0.75$  and  $0.9$ , simulations are also conducted using finer grid models, GT1 and GT2. Table 5 shows a comparison of rotor thrust and torque yielded from different grid models, where  $\Delta_{su}$  is the relative difference between steady and unsteady flow simulation results. The open water performance curves are shown in Figure 8.

**Table 5:** The comparison of steady and unsteady simulations results obtained from different grid models.

$J$	Model ID.	$K_{TR}$			$10K_Q$		
		steady	unsteady	$\Delta_{su}$	steady	unsteady	$\Delta_{su}$
<b>0.75</b>	<b>GT3</b>	0.5209	0.5426	4.0%	0.9996	1.0360	3.5%
	<b>GT2</b>	0.5160	0.5342	3.4%	0.9930	1.0254	3.2%
	<b>GT1</b>	0.5148	0.5321	3.3%	0.9913	1.0221	3.0%
<b>0.9</b>	<b>GT3</b>	0.4938	0.5183	4.7%	0.9654	1.0067	4.1%
	<b>GT2</b>	0.4881	0.5089	4.1%	0.9576	0.9944	3.7%
	<b>GT1</b>	0.4873	0.5059	3.7%	0.9568	0.9897	3.3%



**Figure 8:** Comparison of RANS-simulated and experimental open water performances.



The results shown in Table 4, Table 5, and Figure 8 indicate that

1) The results of steady and unsteady simulations are generally in agreement with physical model experiments. The simulated thrust and torque coefficients are smaller than experimental data at lower  $J$  but higher at larger  $J$ . The simulated efficiency is always higher than the experimental values.

2) The results of  $K_{TR}$ ,  $K_{TT}$  and  $K_Q$  obtained from unsteady flow simulations are all higher than those of steady flow simulations, although the differences between the two flow models become smaller as the grid and time-step sizes decrease.

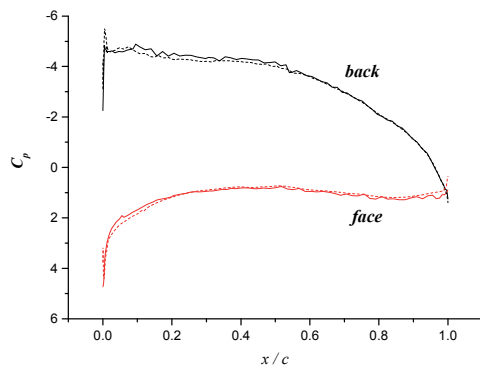
### 4.3 Influence of tip geometry on tip-clearance flow features

Based on the uncertainty analysis and the validation against physical experiments, the grid model GT2 is chosen for investigating the tip-clearance flow. The tip-clearance flow features, such as streamlines and pressure field, and hydrodynamic performance are numerically investigated and compared between PJP-1 and PJP-2 to study the influence of different tip geometries. The unsteady RANS simulations are carried out at  $J=0.75$  and  $J=0.9$ .

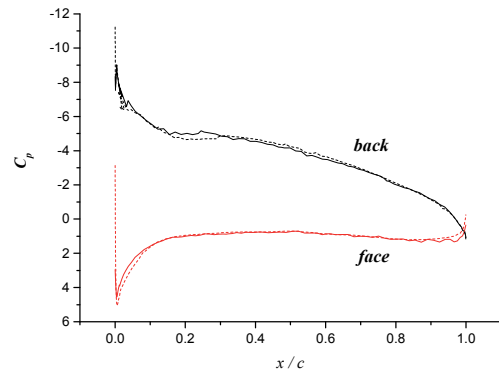
Table 6 compares the simulated rotor thrust and torque, where  $\Delta_{12}$  is the relative difference between results of PJP-1 and PJP-2. Figure 9 shows the pressure distributions at  $r=0.95r_R$  and  $r=0.98r_R$ . As far as PJP-1 and PJP-2 are concerned, the differences in blade-tip geometry seem to have little influence on the open water performance. The pressure distributions near the tip of PJP-2 are a little smoother than those of PJP-1, but the negative pressure peaks of PJP-2 are higher than those of PJP-1.

**Table 6:** Comparison of the simulated hydrodynamic performances of PJP-1 and PJP-2.

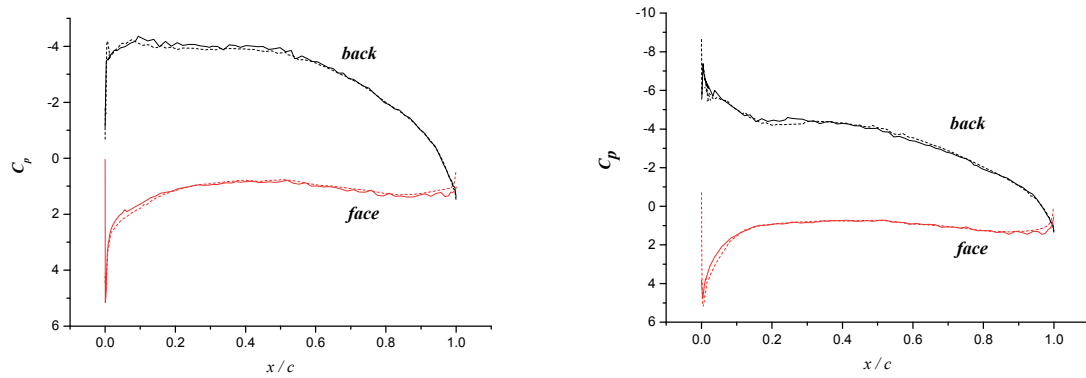
$J$	$K_{TR}$			$10K_Q$		
	PJP-1	PJP-2	$\Delta_{12}$	PJP-1	PJP-2	$\Delta_{12}$
<b>0.75</b>	0.5342	0.5351	0.17%	1.0254	1.0267	0.13%
<b>0.9</b>	0.5089	0.5099	0.18%	0.9944	0.9960	0.15%



(a)  $J=0.75, r/r_R=0.95$



(b)  $J=0.75, r/r_R=0.98$

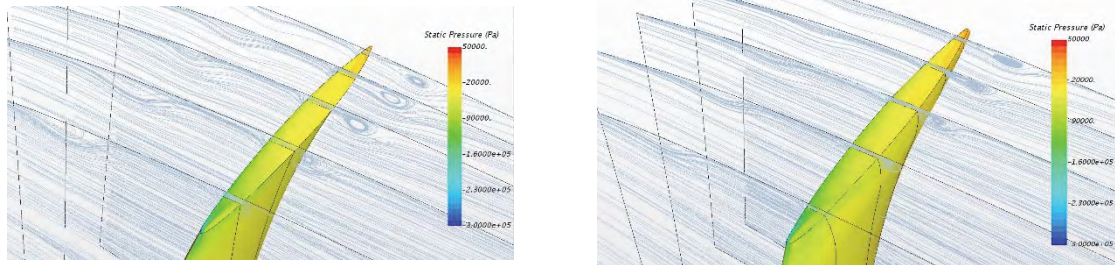


(c)  $J=0.9, r/r_R=0.95$

(d)  $J=0.9, r/r_R=0.98$

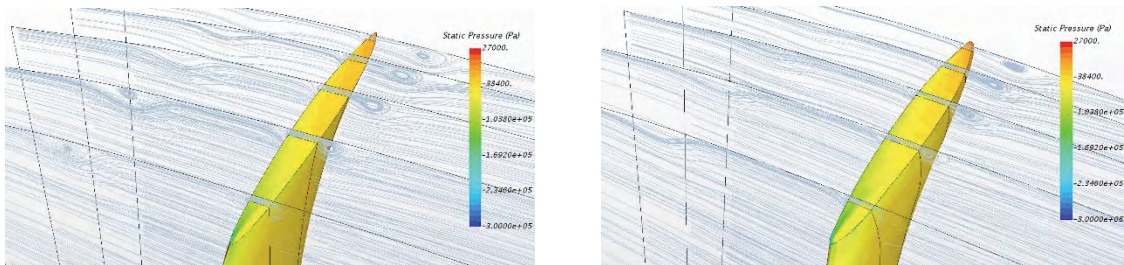
**Figure 9:** Comparison of simulated pressure distributions near the tips of PJP-1 (solid lines) and PJP-2 (dashed lines).

Figure 10 shows the streamlines in the sections perpendicular to the tip chord. The sections are at the position, respectively, 10%, 30%, 50%, 70% and 90% of the tip chord length from the leading edge. A typical static pressure field around the rotor blade tip and streamlines in one section are shown in Figure 11. Compared to PJP-1, the secondary flow in PJP-2 produces stronger detached vortex near the pressure side but weaker tip leakage vortex behind the suction side. The two vortices travel downstream and form a stable tip vortex. It is notable that in the two conditions ( $J=0.75, 0.9$ ), the tip vortex of PJP-2 is obviously weakened in comparison with PJP-1, especially in the sections close to the leading edge.



(a)  $J=0.75, \text{PJP-1}$

(b)  $J=0.75, \text{PJP-2}$



(c)  $J=0.9, \text{PJP-1}$

(d)  $J=0.9, \text{PJP-2}$

**Figure 10:** The streamlines in sections across the tip surface.

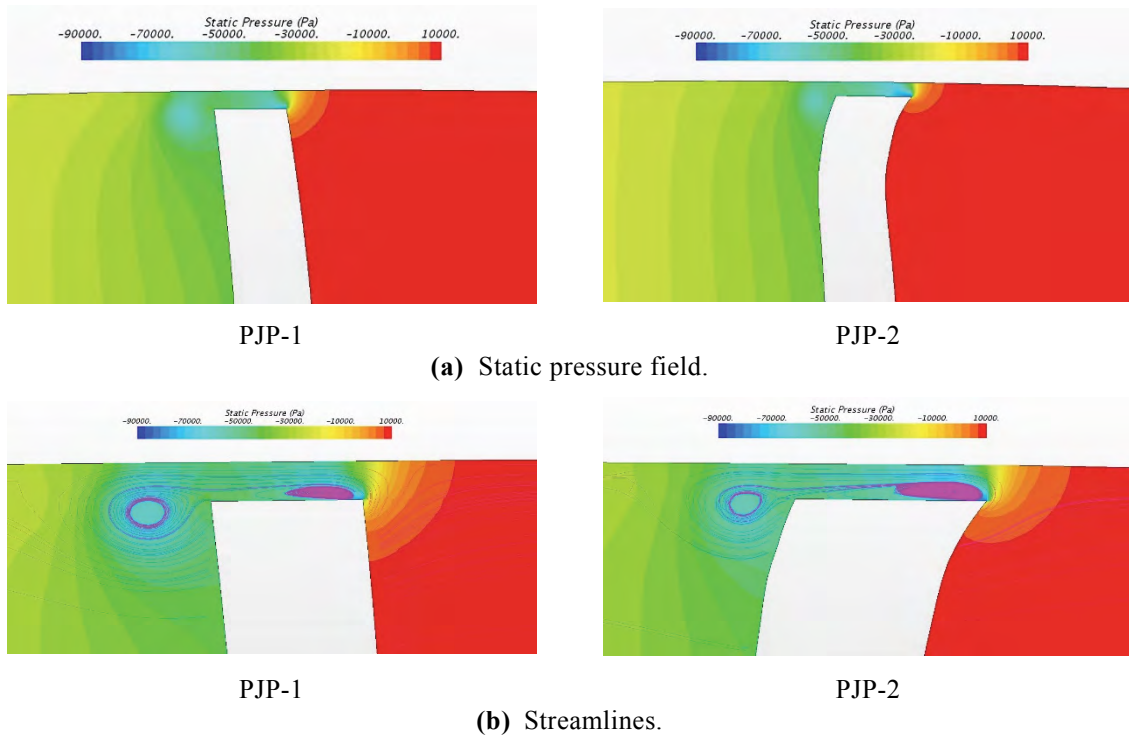


**Figure 11:** The pressure field and streamlines in the section at 30% tip chord length,  $J=0.9$ .

## 5 CONCLUDING REMARKS

In this paper, RANS simulations are carried out to investigate the influence of rotor-tip geometry on the tip-flow features of a pump-jet propulsor. The computational domain is discretized into block-structured hexahedral cells. To evaluate the numerical uncertainties according to the ITTC's recommended procedure, three sets of grids having a uniform refinement ratio are generated, and the unsteady flow simulations are carried out. The validation is generally achieved at the  $U_V$  level of 2.5% to 2.7%. The open water performances obtained from steady and unsteady flow simulations are generally in agreement with physical model experiments. The unsteady simulation results of thrust and torque are all higher than those of steady simulation. The differences between steady and unsteady simulations become smaller as the grid size decreases. The tip-clearance flow features are numerically investigated, with medium grids and time step, for varied profiles of section thickness and rake in the tip region. There is no obvious difference in open water performance and pressure coefficient between PJP-1 and PJP-2. The secondary flow in PJP-2 produces stronger detached vortex near the pressure side but weaker tip leakage vortex behind the suction side. The two vortices travel downstream and form a stable tip vortex. It is notable that the tip vortex of PJP-2 is obviously weakened in comparison with PJP-1, especially in the sections close to the leading edge. A more systematic investigation seems to be necessary in the hope of finding a tip geometry capable of weakening the tip-clearance flow.

## REFERENCES

- [1] Suryanarayana, Ch. Design development and testing of pump-jet propulsor. *NSTL Report*. Visakhapatnam, No. NSTL/SR/136, (1999).
- [2] Suryanarayana, Ch.; Satyanarayana, B. and Ramji, K. Experimental evaluation of pump-jet propulsor for an axisymmetric body in wind tunnel. *International Journal of Naval Architecture and Ocean Engineering* (2010) **2(1)**: 24-33.
- [3] Ivanell, S. Hydrodynamic simulation of a torpedo with pump jet propulsion system. Master thesis, Royal Institute of Technology, Stockholm, 2001.
- [4] Cheah, K.W.; Lee, T.S.; Winoto, S.H. and Zhao, Z.M. Numerical flow simulation in a centrifugal pump at design and off-design conditions. *Int.J.Rotat*(2007).
- [5] Pan, G.; Hu, B.; Wang, P.; Yang, Z.D. and Wang, Y.Y. Numerical simulation of steady hydrodynamic performance of a pump-jet propulsor. *Journal of Shanghai Jiao Tong University* (2013) **47**:932-937.
- [6] Lu, L. and Pan, G. Numerical simulation analysis of unsteady cavitation performance of a pump-jet propulsor. *Journal of Shanghai Jiao Tong University* (2015) **49**:262-268.
- [7] Lu, L.; Gao, Y.F.; Li, Q.; and Du, L. Numerical investigation of tip flow characteristics of a pump-jet propulsor. *International Journal of Naval Architecture and Ocean Engineering* (2018) **10**:307-317.
- [8] Qin, D.H.; Pan, G.; Huang, Q.G.; Zhang, Z.D. and Ke, J.J. Numerical investigation of different tip clearances effect on the hydrodynamic performance of a pump-jet propulsor. *International Journal of Computational Methods* (2018) **15**.
- [9] Gu, L.; Wang, C. and Hu, J. Hydrodynamic performance prediction of a pump jet and impact analysis of a duct camber. *Journal of Harbin Engineering University* (2018) **39**:1752-1758.
- [10] Shimizu, Y.; Yoshikawa, T. and Matsumuru, S. Power augmentation effects of horizontal axis wind turbine by tip vane. *Trans of JSME* (1990) **56(522)**: 495-507.
- [11] Shimizu, Y.; Yoshikawa, T. and Matsumuru, S. Power augmentation effects of horizontal axis wind turbine with a tip vane part1 : Turbine performance and tip vane configuration. *Fluids Eng.*(1994) **116(2)**: 287-292.
- [12] Li, N.; Zhang, L.G.; Wang, Z.L. and Cai, Y.L. Numerical analysis of influence of tip vane width on pulse pressure of pump's shroud. *Noise and Vibration Control* (2014) **34**:34-37.
- [13] Rodi, W. Experience with two-layer models combining the k-epsilon model with a one-equation model near the wall. In Proceedings of the 29th Aerospace Sciences Meeting, Reno, Nevada, (1991).
- [14] Shih, T.H.; Liou, W.W.; Shabbir, A.; Yang, Z. and Zhu, J. A new k-  $\epsilon$  eddy viscosity model for high Reynolds number turbulent flows-model development and validation. *Comput. Fluids* (1995) **24**:227-238.
- [15] ITTC. Uncertainty Analysis in CFD, Verification and Validation Methodology and Procedures. *ITTC-Recommended Procedures and Guidelines*, 7.5-03-01-01. In Proceedings of the International Towing Tank Conference, Wuxi, China (2017).
- [16] Qiu, J.T.; Yang, C.J.; Dong, X.Q.; Wang, Z.L.; Li, W. and Noblesse, F. Numerical simulation and uncertainty Analysis of an axial-flow waterjet pump. *J. Mar. Sci. Eng.*(2018).